FEBS Letters

Crystal structures of Dronpa complexed with quenchable metal ions provide insight into metal biosensor development

In Jung Kim[1], Sangsoo Kim[2], Jeahyun Park[2], Intae Eom[2], Sunam Kim[2], Jin-Hong Kim[2], Sung Chul Ha[2], Yeon Gil Kim[2], Kwang Yeon Hwang[1] and Ki Hyun Nam[2]

1 Division of Biotechnology, College of Life Sciences & Biotechnology, Korea University, Seoul, Korea
2 Pohang Accelerator Laboratory, Pohang University of Science and Technology, Korea

Correspondence
K. Y. Hwang, Division of Biotechnology, College of Life Sciences & Biotechnology, Korea University, Seoul 136-701, Korea
Fax: 82 2 923 3225
Tel: 82 2 3290 3009
E-mail: chahong@korea.ac.kr
and
K. H. Nam, Pohang Accelerator Laboratory, Pohang, Kyungbuk 790-784, Korea
Fax: 82 54 279 1599
Tel: 82 54 279 1187
E-mail: structure@postech.ac.kr

(Received 15 April 2016, revised 27 June 2016, accepted 11 July 2016)

doi:10.1002/1873-3468.12316

Edited by Richard Cogdell

Many fluorescent proteins (FPs) show fluorescence quenching by specific metal ions, which can be applied towards metal biosensor development. In this study, we investigated the significant fluorescence quenching of Dronpa by Co^{2+} and Cu^{2+} ions. Crystal structures of Co^{2+}-, Ni^{2+}- and Cu^{2+} -bound Dronpa revealed previously unseen, unique, metal-binding sites for fluorescence quenching. These metal ions commonly interact with surface-exposed histidine residues (His194-His210 and His210-His212), and interact indirectly with chromophores. Structural analysis of the Co^{2+}- and Cu^{2+}- binding sites of Dronpa provides insight into FP-based metal biosensor engineering.

Keywords: biosensor; Dronpa; fluorescent protein; metal-binding site; quenching

Metal ions are required for the proper function of all living organisms and act as catalysts in cells, enzyme stabilizers and regulators of gene expression and membrane osmotic pressure [1,2]. Small doses of heavy metals (including cobalt, copper, iron, manganese, molybdenum, vanadium, strontium and zinc) are essential for a healthy life; however, excessive levels of metal ions can affect human biological processes such as ageing and disease development [1]. In order to measure metal ions levels, various metal biosensors have been reported using peptides, proteins, enzymes, antibodies, whole cells and nucleic acids [3–7].

Fluorescent proteins (FPs) are popular optical markers and represent molecules with spatial and temporal specificity towards applications in medicine, as well as molecular and cell biology [8]. One of the interesting properties of FPs is fluorescence quenching by specific divalent metal ions [9,10]. Many fluorescent proteins have been used for biosensing applications to detect transition metal ions [11–16]. For instance, DsRed from a reef coral has been reported as a copper sensor with highly selective, reversible and sensitive detection capacities for both Cu^{+} and Cu^{2+}, and a detection limit in the nanomolar range [12,17]. In the enhanced green fluorescent protein (EGFP), surface-exposed S202 and Q204 residues were mutated into histidine residues that bind copper over 200-folds stronger than wild-type EGFP [18]. The jellyfish *Aequorea victoria* mutant Green Fluorescent Protein (GFP) (eGFP205C, S205C) has been employed to develop highly specific

Abbreviations
EGFP, enhanced green fluorescent protein; FPs, fluorescent proteins.

and noninvasive biosensors towards mercury ions and used for an *in vivo* application in *Escherichia coli* [19]. Change in fluorescence which metal ions produce can occur either by static quenching, energy transfer between binding metal and the chromophore, or perturbations of the protein structure [9,13,20]. In particular, the presence of metal ions in the close vicinity of a chromophore induces the fluorescence quenching in a distance-dependent fashion [9,21].

Although many FPs have been biochemically characterized in terms of their quenching effect by metal ions, only two metal-bound structures have been reported to date. In BFPms1 (mutant GFP from *Aequorea victoria)*, a point mutation (H148G) was introduced in the β-barrel surface in order to improve the metal-binding kinetics and generate a solvent-accessible channel [11]. Cu^{2+} (quenching fluorescence) and Zn^{2+} (enhancing fluorescence intensity) ions accessed the vicinity of chromophore to interact with it [11]. In iq-mEmerald, the two engineered surface-exposed histidine residues in a β-sheet (*i* and *i* + 2) created a binding site for transition metals [22]. Cu^{2+} ion induced the quenching of the fluorescence intensity, whereas other metal ions generated little reduction (Co^{2+}) or enhancement (Zn^{2+} and Ni^{2+}) of the fluorescence activity [23]. Iq-mEmerald crystal structures complexed with Ni^{2+} and Zn^{2+} ions showed that both metal ions interact with engineered histidine residues, consisting of indirect interactions of metal ions with the chromophore [23]. Although these structures provide a framework to help understand the metal-binding site and fluorescence effects, indirect interactions between quenchable metal ions and chromophores have not been determined yet. Dronpa is a reversibly photoswitchable green fluorescent protein from *Echinophyllia* sp. SC22, with which the monitoring of fast protein dynamics, such as nucleocytoplasmic shuttling of a signalling protein, becomes possible *in vivo* [24].

In this study, we investigate the fluorescence quenching effect of Dronpa by transition metal ions. The crystal structures of Dronpa complexed with Co^{2+}, Ni^{2+} and Cu^{2+} reveal previously unseen metal-binding sites and their distinct configurations. Our structural results provide insight into the design of engineered FP-based metal biosensors.

Materials and methods

Sample preparation

The cloning and expression of Dronpa (C62S) was performed as described previously [25]. The final purified protein was kept in 10 mM Tris-HCl and 50 mM NaCl.

Metal ion screening and titration of Dronpa

The examination of the metals' effects on Dronpa were carried out introducing the 10 μM Dronpa in a 200 μL reaction volume together with the 1 mM metal ions ($MgCl_2$, $CaCl_2$, $MnCl_2$, $CoCl_2$, $NiCl_2$, $CuCl_2$ and $ZnCl_2$). Initial fluorescent quenching was observed using the ultra-bright LED transilluminator at 470 nm. Next, the fluorescence quenching was performed at 26 °C for 5 min in the reaction mixture containing 10 μM Dronpa and 50 or 100 μM of metal ions, such as $MgCl_2$, $CaCl_2$, $MnCl_2$, $CoCl_2$, $NiCl_2$, $CuCl_2$ and $ZnCl_2$ in a total volume of 100 μL. Fluorescence emission quantum yields were measured with Infinite 200 Pro microplate reader (TECAN) using a 483-nm filter for excitation and a 535-nm filter for emission. The titration experiments of 10 μM Dronpa were carried out for 0.78–400 μM $CoCl_2$ and $CuCl_2$. To test the reversibility of the fluorescence quenching, 100 μM EDTA was added to the quenched Dronpa containing 100 μM $CoCl_2$ and $CuCl_2$. All experiments were performed in triplicate.

Crystallization, diffraction data collection and refinement

Dronpa was crystallized at 10 $mg{\cdot}mL^{-1}$ in 50 mM Tris-HCl, pH 8.5, 200 mM $MgCl_2$, and 10% (w/v) PEG 4000, and it was equilibrated at 22 °C using the hanging drops vapour diffusion method. For crystal protection, crystals were immersed in the stabilizing solution implemented with 20% (w/v) ethylene glycol, and added at a final concentration of 0.1 mM in $CoSO_4$, $NiSO_4$ or $CuSO_4$ for 5 min before flash freezing in a gaseous liquid nitrogen stream. X-ray diffraction data were collected at the beamline 7A at PLS-II (Pohang, Korea) using Quantum 210 CCD (ADSC). Data sets were indexed and reduced in the P1 space group with the HKL2000 program [26].

Structure determination and analysis

The phases were obtained by molecular replacement with MOLREP [27] and Dronpa-C62S (PDB code 2GX2) as an initial model [25]. The model building and refinement was done using the COOT program [28], and refined in REFMAC5 [29]. The final structures were validated by MOLPROBITY [30]. Data collection and structure refinement statistics are shown in Table 1. The structure-based sequence alignment was carried out using ClustalW and ESPript [31,32]. Temperature B-factor distributions were analysed using CCP4 [33]. The structure figures were prepared using the PYMOL program (Schrödinger, LLC). The final coordinates and structure factors have been deposited within the Protein Data Bank under the accession codes 5HZS (Dronpa-Co^{2+}), 5HZT (Dronpa-Cu^{2+}), and 5HZU (Dronpa-Ni^{2+}).

Table 1. Data collection and refinement statistics for Dronpa-metal complexes

	Dronpa-Co^{2+}	Dronpa-Ni^{2+}	Dronpa-Cu^{2+}
Data collection			
Space group	P1	P1	P1
Cell dimensions			
a, *b*, *c* (Å)	72.3, 105.5, 109.8	105.4, 109.4, 72.1	72.4, 105.9, 108.0
α, β, γ (°)	115.8, 109.5, 93.9	71.1, 85.9, 61.3	115.9, 107.7, 94.1
Resolution (Å)	30.0–2.20 (2.24–2.20)	30.0–1.90 (1.93–1.90)	30.0–2.85 (2.95–2.85)
Completeness	95.1 (92.9)	94.9 (90.5)	93.6 (83.6)
Redundancy	3.1 (2.8)	3.0 (2.4)	2.9 (2.1)
$I/\sigma(I)$	25.0 (4.04)	22.1 (3.05)	19.2 (2.88)
R_{merge} (%)[a]	7.5 (30.4)	7.7 (36.4)	8.8 (33.9)
Refinement statistics			
Resolution (Å)	30.0–2.20	30.0–1.90	30.0–2.85
R_{work}/R_{free} (%)[b]	16.88/22.53	15.34/19.93	21.56/24.50
B-factor (Averaged)			
Protein	31.15	23.70	56.88
Metal ions	48.20	36.31	90.78
Water	33.46	31.23	34.73
R.m.s deviations			
Bond lengths (Å)	0.019	0.019	0.019
Bond angles (°)	1.961	1.961	1.960
Estimated overall coordinate error (Å)[c]	0.155	0.093	0.321
Ramachandran plot (%)			
Favoured	97.9	99.0	98.3
Allowed	2.1	1.0	1.7

Highest resolution shell is shown in parentheses.

[a] $R_{merge} = \sum_h \sum_i |I_i(hkl) - \langle I(hkl)\rangle| / \sum_h \sum_i I_i(hkl)$, where $I_i(hkl)$ is the intensity of the 'ith' measurement of reflection hkl and $\langle I(hkl)\rangle$ is the weighted mean of all measurements of hkl.

[b] $R_{work} = \sum||F_{obs}| - |F_{calc}|| / \sum|F_{obs}|$, where F_{obs} and F_{calc} are the observed and calculated structure-factor amplitudes respectively. R_{free} was calculated as R_{work} using a randomly selected subset (10%) of unique reflections not used for structure refinement.

[c] Estimated based on Maximum Likelihood Method.

Results and Discussion

Fluorescence quenching of Dronpa by Co^{2+} and Cu^{2+}

To investigate the metal-induced fluorescence quenching of Dronpa, the purified protein was incubated in $MgCl_2$, $CaCl_2$, $MnCl_2$, $CoCl_2$, $NiCl_2$, $CuCl_2$ or $ZnCl_2$ solution. The mixture product was initially visualized with LED transilluminator at 470 nm (Fig. 1A). Cu^{2+} and Co^{2+} ions strongly reduced the fluorescent intensity, whereas the other metal ions showed similar intensities to apo-Dronpa. To confirm the metal effects, the fluorescence emissions at 535 nm of the mixed samples were measured. Co^{2+} and Cu^{2+} clearly exerted the strongest quenching effect on the fluorescence intensity of Dronpa (Fig. 1B and Table S1); 50 μM Co^{2+} and Cu^{2+} quenched the fluorescence intensity by 26% and 86%, respectively, and 100 μM Ni^{2+} also slightly reduced the fluorescence emission by 6.3% (Fig. 1B). However, Mg^{2+}, Ca^{2+}, Mn^{2+} and Zn^{2+} enhanced the fluorescence emission of Dronpa. Looking at metal dependence, we revealed that Dronpa quenching could be enhanced by various extents, depending on the different divalent metal ions present, in the following descending order: $Cu^{2+} > Co^{2+} \gg Ni^{2+} < Mg^{2+}$, Ca^{2+}, Zn^{2+} and Mn^{2+} (Fig. 1B). Next, we investigated the effect of increasing Cu^{2+} and Co^{2+} concentrations (0.78–400 μM) on Dronpa. Fluorescence intensity of Dronpa significantly dropped in ~ 25 μM Co^{2+} and ~ 6.25 μM Cu^{2+} solutions (Fig. 1C,D and Table S2). Co^{2+} and Cu^{2+} displayed reversibility capacities of ~ 97% and ~ 95%, respectively, after addition of the metal ion chelator (EDTA) (Fig. S1 and Table S3). This result indicates that Cu^{2+} and Co^{2+} bind to the surface of the β-barrel of Dronpa, because the EDTA molecule could not access the internal area of the Dronpa β-barrel (Fig. S2). Overall, these results show that Dronpa can be used as a sensitive fluorescent probe towards the detection of both Co^{2+} and Cu^{2+} ions.

Overall structure of the metal-bound Dronpa

In order to identify the metal-binding sites, we determined the crystal structures of Dronpa complexed with

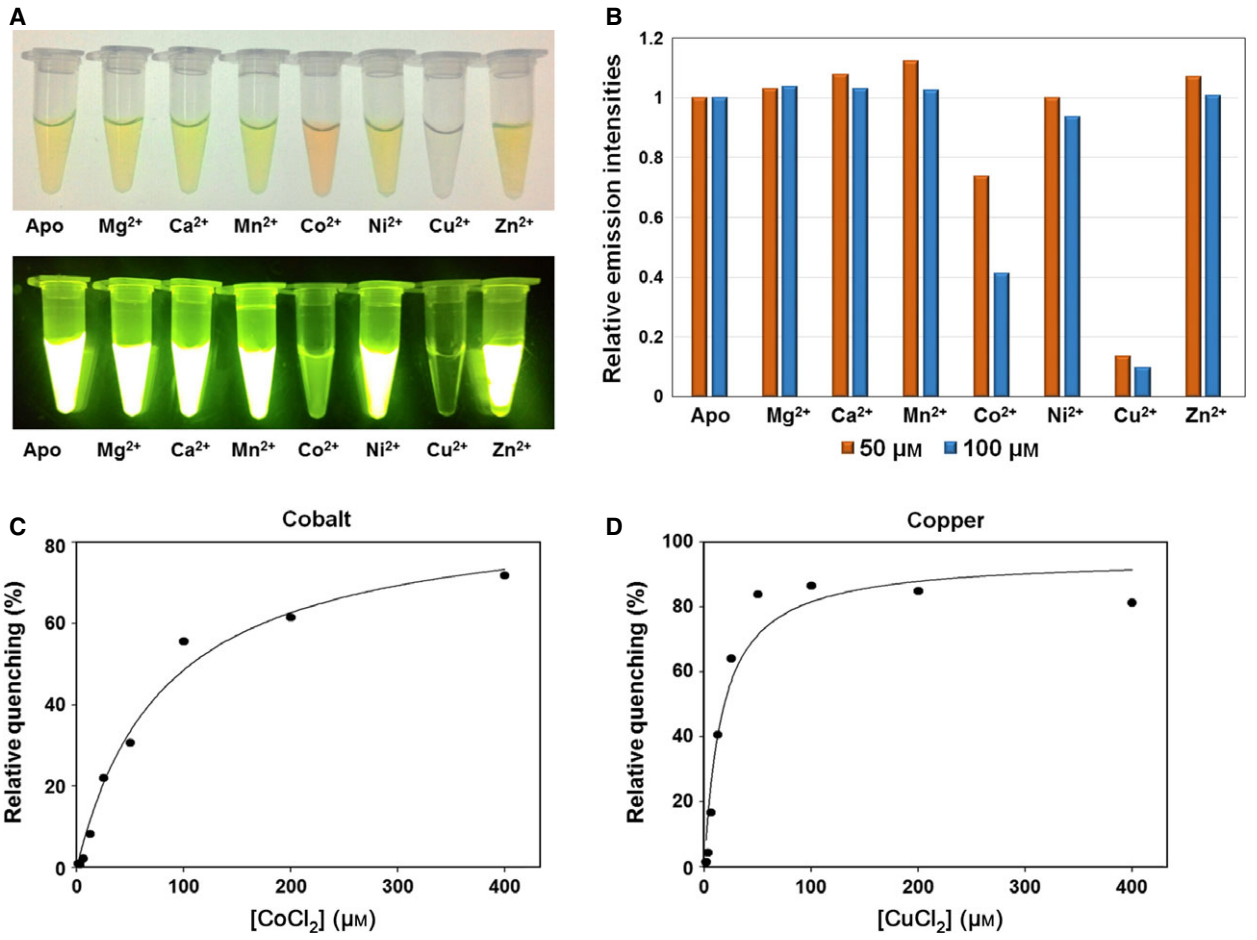

Fig. 1. Highly sensitive fluorescence quenching of Dronpa by Cu^{2+} and Co^{2+} ions. (A) Visualization of the fluorescence quenching by metal ions. 10 μM Dronpa was incubated with 1 mM divalent metal ions (Ca^{2+}, Mg^{2+}, Mn^{2+}, Co^{2+}, Ni^{2+}, Cu^{2+} and Zn^{2+}). The fluorescence intensities were visualized using the LED transilluminator at 470 nm (B) Quenching effect of metal ions on Dronpa fluorescence. Relative emission intensities of Dronpa with and without 50 or 100 μM metal ions. Co^{2+} and Cu^{2+} ions significantly induced the fluorescence quenching of Dronpa. (C, D) Titration of the Dronpa with Co^{2+} and Cu^{2+} ions. Emission spectra of Dronpa were measured at 538 nm, in the presence of 0.78–400 μM metal ions. The data set (line) were fitted to the hyperbolic equation.

Co^{2+}, Ni^{2+} and Cu^{2+}. All crystals belonged to the triclinic P1 space group with twelve molecules occupying the asymmetric unit. The conformational differences between the Dronpa molecules are shown in Table S4–S6**.** Upon structure determination, the spherical strong peaks of density at > 5 σ in the different Dronpa F_o–F_c simulated annealing omit maps clearly showed where the metal ions are binding (Fig. S3). Co^{2+}, Cu^{2+} and Ni^{2+} commonly interact with surface-exposed histidine residues on the external surface of the β-barrel, in vicinity of the chromophore (Fig. 2).

The binding sites of Co^{2+} and Ni^{2+} are positioned within the same location, whereas that of Cu^{2+} is located at a distinct position (Fig. 2A). Both Co^{2+} and Ni^{2+} are 14.4 ((standard deviation for 12 monomers in the ASU: 10) for Co^{2+} and (4) for Ni^{2+}) Å and 11.5 ((16) for Co^{2+} and (10) for Ni^{2+}) Å away from the centre of the imidazolinone and tyrosine rings in the chromophore respectively. Based on the perpendicular view of the chromophore, Co^{2+} and Ni^{2+} are rotated 10.5° counterclockwise from the vertical axis pointing from the imidazolinone ring of the chromophore (Fig. 2B). At an equivalent position, Cu^{2+} is 14.7 (14) Å and 14.4 (22) Å away from the chromophore rings and is rotated 18.5° clockwise (Fig. 2B). A previously published study measured the distances of intact energy transfer between the quenchable metal ions (FRET donor) and the chromophores (FRET accept) by using FRET measurements [23]. The FRET-specific signals of fluorescent proteins (EBFP2, mCeruleans3, iq-mEmerald, mVenus, mApple and mKate2) revealed an average distance of 12.2 Å (distance range was approximately 7–19 Å)

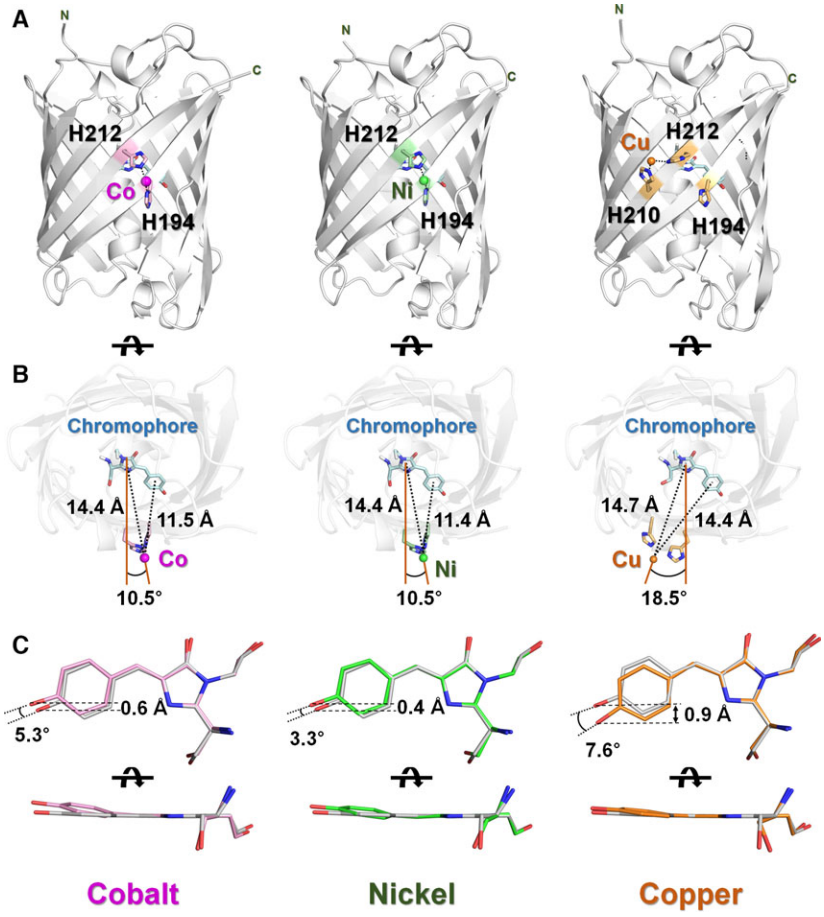

Fig. 2. Overall structures of Co^{2+}-, Ni^{2+}- and Cu^{2+}-bound Dronpa. (A) Metal-binding sites for the Co^{2+}, Ni^{2+} and Cu^{2+} on Dronpa. (B) Distances and angles between metal ions and chromophores (measured from centers of the imidazolinone and tyrosine rings). (C) Conformational change in the chromophore by Co^{2+} (pink), Ni^{2+} (green) and Cu^{2+} (orange) ions. Conformational change for the distance angle of each chromophore was compared with that of apo-Dronpa (grey, PDB ID: 2GX2). Binding of Co^{2+} and Ni^{2+} show relatively similar structural properties, whereas that of Cu^{2+} displays a distinct configuration.

between the metal ions and the chromophores [23]. The distances of the metal ions from the chromophore for Dronpa are within the range of the distances for the other metal-bound FPs determined by FRET measurements [23]. The overall structures showed similarities with the apo-Dronpa structure (PDB ID: 2GX2) with r.m.s. deviations of less than 0.238 Å for all Cα atoms (Fig. S4A). However, the metal-bound Dronpa displayed small conformational changes within the chromophores compared with apo-Dronpa (Fig. S4B). Regarding the alignment of the imidazolinone ring in chromophores, the tyrosine residue shows tilting and shifting by Co^{2+} (average tilt angle and shift: 5.4° (11) and 0.58 (9) Å), Ni^{2+} 3.4° (10) and 0.47 (12) Å), and Cu^{2+} 7.6° (19) and 0.95 (17) Å) (Fig. 2C). Moreover, the environment of the chromophores showed small conformational changes (Fig. S5).

Co^{2+}-, Ni^{2+}- and Cu^{2+}-binding sites

For Co^{2+} and Ni^{2+}, both metal-binding sites are located on the external surface between β10- and β11-stands and show distorted octahedral coordination (Fig. 3A,B). Co^{2+} was found coordinated by Nδ atom of His194 (average distance of 2.21 (15) for 12 molecules in the ASU), Nε atom of His212 (2.26 (10) Å), and four water molecules (2.20 (13) Å) (Fig. 3A). Ni^{2+} also shows coordination with the Nδ atom of His194 (2.12 (6) Å), Nε atom of His212 (2.19 (7) Å), and four water molecules (2.25 (7) Å) (Fig. 3B and Table S6). In general, Co^{2+} and Ni^{2+} ions favour an octahedral arrangement over the square planar coordination [34]. This indicates that Co^{2+} and Ni^{2+} in Dronpa displayed typical metal-binding geometry, whereas the water molecules, in distorted octahedral coordination, showed a different configuration (Fig. S6). The Co^{2+}- and Ni^{2+}-binding positions revealed similar patterns; however, biochemical results showed that Co^{2+} ions reduced the fluorescence emission of Dronpa more than Ni^{2+} ions (Fig. 1B). We consider that the energy transfer between chromophores and metal ions (Co^{2+} and Ni^{2+}) could involve mechanisms such as surface energy transfer (SET) and electron transfer [35]. These energy transfer processes between chromophores (donor) and

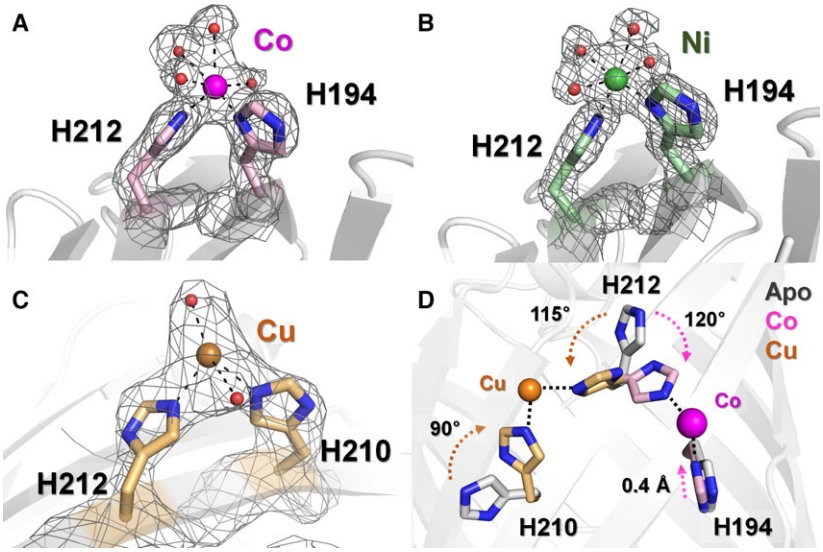

Fig. 3. Co^{2+}-, Ni^{2+}- and Cu^{2+}-binding sites. Metal-binding site of the Dronpa complexed with (A) Co^{2+}, (B) Ni^{2+} and (C) Cu^{2+}. A $2F_o$-F_c electron density maps are shown in grey for the Co^{2+} (contoured at 1.5 σ), Ni^{2+} (1.5 σ), and Cu^{2+} (1.2 σ) around the binding residues, metal ions and water molecules. (D) Conformational change in metal-binding residues of apo-Dronpa (grey) by Co^{2+} (pink) and Cu^{2+} (orange) ions. Co^{2+} ion induced conformational changes of His194 and His212 side chains. Changes for Ni^{2+}, identical to those for Co^{2+}, were omitted in this figure for clarity. Cu^{2+} ion induced conformational changes of His210 and His212 side chains.

metal ions (acceptor) are dependent on the physical and chemical characteristics of the specific metal ions [35]. In Cu^{2+}-Dronpa, the metal ion is located on the β12-strand and coordinated with the Nδ atom of His210 (2.34 (23) Å), Nε atom of His212 (2.54 (33) Å) (Fig. 3C and Table S6). The histidine residues and Cu^{2+} were well defined in the electron density map (Fig. S3), which was not the case for the water molecules (Fig. 3C). Particularly, the amino acid sequence of His210 and His212 (*i* and *i* + 2) on the β12-strand of Dronpa was identical to that previously reported in robust transition metal binding in a β-sheet mode [22,23]. Many FPs have shown Cu^{2+}-induced fluorescence quenching [12–15,17,18,23], but the configuration of the Cu^{2+} binding was still unknown. Thus, determination of the Cu^{2+}-binding site in Dronpa could be useful to understand other Cu^{2+} sensitive FPs.

Superimposition of the apo- and metal-bound structures shows conformational changes of the side chains of metal interacting histidine residues in Co^{2+}-, Ni^{2+}- and Cu^{2+}-Dronpa complexes (Fig. 3D). With Co^{2+} and Ni^{2+}, the imidazole side chain in His194 residues was rotated by ~ 180° and moved towards the metal ion with a small positional shift of 0.4–0.6 Å. The side chain of His212 was rotated by ~ 120° (Fig. 3D). In Cu^{2+}, both imidazole side chains in His210 and His212 were flipped towards the metal site by ~ 90° and ~ 115° respectively (Fig. 3D).

Comparison with other FP-based biosensors

In order to explore the conservation of metal-binding sites, Dronpa and previously reported metal-bound FPs were compared (Fig. 4). In iq-mEmerald, Zn^{2+} and Ni^{2+} ions interact with two surface-exposed engineered His202 and His204 residues (Fig. 4A) [23]. These engineered histidine residues are based on previously reported robust transition metal-binding modes (*i* and *i* + 2) on a β-sheet [9]. This latter feature makes iq-mEmerald a common candidate for the development of FP-based metal biosensors [23]. A structural comparison shows that metal-binding modes (*i* and *i* + 2) on a β-sheet of Dronpa and iq-mEmerald are located at β12- and β11-strands (numbers as in Dronpa) respectively (Fig. 4A,E). This finding of a unique Cu^{2+}-binding site by His210 and His212 on a β12-strand in Dronpa could provide insight into a new engineering pathway for the development of FP-based copper biosensors (Fig. 4E). Ni^{2+} is not a suitable metal ion for fluorescence quenching of both Dronpa and iq-mEmerald, whereas Co^{2+} shows the most sensitive quenching of fluorescence emission [23]. The Co^{2+}-binding site of iq-mEmerald has not yet been determined. The crystal structures of metal-bound Dronpa display identical metal-binding sites for both Ni^{2+} and Co^{2+} (Figs 2 and 3). Although the configuration of the Ni^{2+}-binding residues of Dronpa and

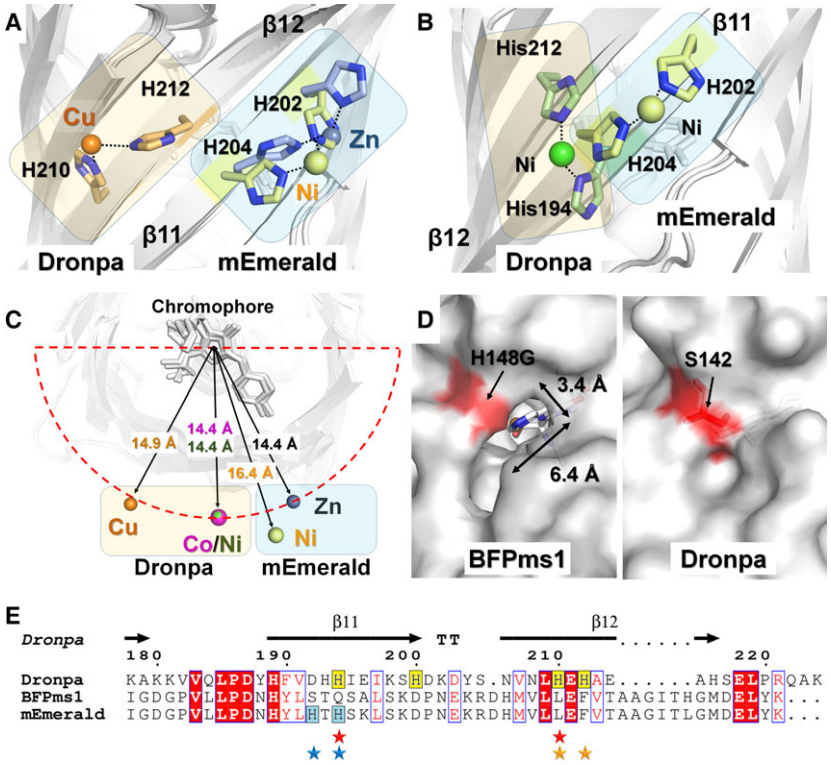

Fig. 4. Comparison of the Dronpa metal-binding sites with iq-mEmerald and BFPms1. (A) The robust metal-binding modes in a β-sheet (i and i + 2) in Dronpa and iq-mEmerald (PDB ID: 4KW4 for zinc and 4KW9 for nickel) are located on the β12- and β11-strands respectively. (B) Comparison of the Ni^{2+}-binding site of Dronpa and iq-mEmerald showing distinct binding configurations through surface-exposed histidine residues. (C) Crystal structures of Dronpa and iq-mEmerald show similarities in the distance between the ion and the chromophore (the centre of the imidazolinone ring). (D) Alignment of the solvent-accessible channel of the BFPm1 (PDB ID: 1KYR for Cu) with Dronpa. The BFPm1 (GFP mutant) has a solvent-accessible channel between the β8- and β9-strand with dimensions of 3.4 × 6.4 Å, whereas Dronpa displays a closed form at an equivalent position. (E) Partial sequence alignment of Dronpa with BFPms1 and mEmerald. The metal-binding sites of Dronpa (red for Co^{2+} and Ni^{2+}, yellow for Cu^{2+}) and mEmerald (blue) are indicated by asterisks.

iq-mEmerald revealed different features (Fig. 4B), Co^{2+}-binding site in iq-mEmerald could be shared with Ni^{2+}-binding site, based on our results. The superimposition of the chromophore of Dronpa and iq-mEmerald showed distinct metal positions, whereas the distances between metal ions and imidazolinone in chromophores revealed similarities in terms of range (14.4–16.4 Å) (Fig. 4C). In BFPms1, the H148G mutant generates a solvent-accessible channel with cross-dimensions of approximately 3.4 × 6.4 Å [11]. Using this channel, Zn^{2+} and Cu^{2+} access the chromophores, where they interact with a dipyrrole unit of a porphyrin. In Dronpa, no solvent-accessible channel is observed at an equivalent position, which is being closed by the hydrogen bond of the main chains between β8- and β9-strands (Fig. 4D).

In summary, Dronpa has shown sensitive and reversible fluorescence quenching by Co^{2+} and Cu^{2+}. The most striking finding are the previously unseen, unique metal-binding sites for the Co^{2+}, Ni^{2+} and Cu^{2+} in Dronpa, which provide an insight into the engineering of other FPs, towards the development of metal biosensors. The fluorescence quenching of Dronpa by Co^{2+} and Cu^{2+} could be utilized for metal biosensor applications, however, two metal-binding sites (His194–His212 and His210–His212) in Dronpa could cause nonspecific metal binding during the detection process. In that regard, site-directed mutagenesis of the His194 or His210 residues of Dronpa is required to improve the specificity towards Co^{2+} or Cu^{2+} binding.

Acknowledgements

We thank the beamline staff at the MX beamlines at PLS-II at Pohang Acceleratory Laboratory for assistance in data collection. IJK is grateful for a grant from

Korea University. This work was supported by the National Research Foundation of Korea (NRF) grant funded by the Korea government (MEST) (NRF-2014R1A1A2059440 and 2013R1A1A2008404).

Author contributions

IJK performed the biochemical studies. SK, JP, JK, SCH and YGK collected diffraction data. IE, SK and KHN determined the structure. KYH and KHN designed the research. IJK, KYH and KHN wrote the manuscript.

References

1 Futra D, Heng LY, Ahmad A, Surif S and Ling TL (2015) An optical biosensor from green fluorescent *Escherichia coli* for the evaluation of single and combined heavy metal toxicities. *Sensors* **15**, 12668–12681.
2 Domaille DW, Que EL and Chang CJ (2008) Synthetic fluorescent sensors for studying the cell biology of metals. *Nat Chem Biol* **4**, 168–175.
3 Mehta J, Bhardwaj SK, Bhardwaj N, Paul AK, Kumar P, Kim KH and Deep A (2016) Progress in the biosensing techniques for trace-level heavy metals. *Biotechnol Adv* **34**, 47–60.
4 Liu Q, Cai H, Xu Y, Xiao L, Yang M and Wang P (2007) Detection of heavy metal toxicity using cardiac cell-based biosensor. *Biosens Bioelectron* **22**, 3224–3229.
5 Bontidean I, Ahlqvist J, Mulchandani A, Chen W, Bae W, Mehra RK, Mortari A and Csoregi E (2003) Novel synthetic phytochelatin-based capacitive biosensor for heavy metal ion detection. *Biosens Bioelectron* **18**, 547–553.
6 Krawczynski vel Krawczyk T, Moszczynska M and Trojanowicz M (2000) Inhibitive determination of mercury and other metal ions by potentiometric urea biosensor. *Biosens Bioelectron* **15**, 681–691.
7 Wang Y, Yang F and Yang X (2010) Colorimetric detection of mercury(II) ion using unmodified silver nanoparticles and mercury-specific oligonucleotides. *ACS Appl Mater Interfaces* **2**, 339–342.
8 Zimmer M (2002) Green fluorescent protein (GFP): applications, structure, and related photophysical behavior. *Chem Rev* **102**, 759–781.
9 Richmond TA, Takahashi TT, Shimkhada R and Bernsdorf J (2000) Engineered metal binding sites on green fluorescence protein. *Biochem Biophys Res Commun* **268**, 462–465.
10 Ibraheem A and Campbell RE (2010) Designs and applications of fluorescent protein-based biosensors. *Curr Opin Chem Biol* **14**, 30–36.
11 Barondeau DP, Kassmann CJ, Tainer JA and Getzoff ED (2002) Structural chemistry of a green fluorescent protein Zn biosensor. *J Am Chem Soc* **124**, 3522–3524.
12 Eli P and Chakrabartty A (2006) Variants of DsRed fluorescent protein: development of a copper sensor. *Protein Sci* **15**, 2442–2447.
13 Isarankura-Na-Ayudhya C, Tantimongcolwat T, Galla HJ and Prachayasittikul V (2010) Fluorescent protein-based optical biosensor for copper ion quantitation. *Biol Trace Elem Res* **134**, 352–363.
14 Hotzer B, Ivanov R, Altmeier S, Kappl R and Jung G (2011) Determination of copper(II) ion concentration by lifetime measurements of green fluorescent protein. *J Fluoresc* **21**, 2143–2153.
15 Masullo T, Puccio R, Di Pierro M, Tagliavia M, Censi P, Vetri V, Militello V, Cuttitta A and Colombo P (2014) Development of a biosensor for copper detection in aqueous solutions using an Anemonia sulcata recombinant GFP. *Appl Biochem Biotechnol* **172**, 2175–2187.
16 Frommer WB, Davidson MW and Campbell RE (2009) Genetically encoded biosensors based on engineered fluorescent proteins. *Chem Soc Rev* **38**, 2833–2841.
17 Sumner JP, Westerberg NM, Stoddard AK, Hurst TK, Cramer M, Thompson RB, Fierke CA and Kopelman R (2006) DsRed as a highly sensitive, selective, and reversible fluorescence-based biosensor for both Cu(+) and Cu(2+) ions. *Biosens Bioelectron* **21**, 1302–1308.
18 Peterffy JP, Szabo M, Szilagyi L, Lanyi S and Abraham B (2015) Fluorescence of a histidine-modified enhanced green fluorescent protein (EGFP) effectively quenched by copper(II) ions. Part II. Molecular determinants. *J Fluoresc* **25**, 871–883.
19 Chapleau RR, Blomberg R, Ford PC and Sagermann M (2008) Design of a highly specific and noninvasive biosensor suitable for real-time in vivo imaging of mercury (II) uptake. *Protein Sci* **17**, 614–622.
20 Mizuno T, Murao K, Tanabe Y, Oda M and Tanaka T (2007) Metal-ion-dependent GFP emission in vivo by combining a circularly permutated green fluorescent protein with an engineered metal-ion-binding coiled-coil. *J Am Chem Soc* **129**, 11378–11383.
21 Cubitt AB, Heim R, Adams SR, Boyd AE, Gross LA and Tsien RY (1995) Understanding, improving and using green fluorescent proteins. *Trends Biochem Sci* **20**, 448–455.
22 Taraska JW, Puljung MC, Olivier NB, Flynn GE and Zagotta WN (2009) Mapping the structure and conformational movements of proteins with transition metal ion FRET. *Nat Methods* **6**, 532–537.
23 Yu X, Strub MP, Barnard TJ, Noinaj N, Piszczek G, Buchanan SK and Taraska JW (2014) An engineered palette of metal ion quenchable fluorescent proteins. *PLoS One* **9**, e95808.

24 Ando R, Mizuno H and Miyawaki A (2004) Regulated fast nucleocytoplasmic shuttling observed by reversible protein highlighting. *Science* **306**, 1370–1373.
25 Nam KH, Kwon OY, Sugiyama K, Lee WH, Kim YK, Song HK, Kim EE, Park SY, Jeon H and Hwang KY (2007) Structural characterization of the photoswitchable fluorescent protein Dronpa-C62S. *Biochem Biophys Res Commun* **354**, 962–967.
26 Otwinowski Z and Minor W (1997) Processing of X-ray diffraction data collected in oscillation mode. *Method Enzymol* **276**, 307–326.
27 Vagin A and Teplyakov A (2010) Molecular replacement with MOLREP. *Acta Crystallogr D Biol Crystallogr* **66**, 22–25.
28 Emsley P, Lohkamp B, Scott WG and Cowtan K (2010) Features and development of Coot. *Acta Crystallogr D Biol Crystallogr* **66**, 486–501.
29 Winn MD, Murshudov GN and Papiz MZ (2003) Macromolecular TLS refinement in REFMAC at moderate resolutions. *Methods Enzymol* **374**, 300–321.
30 Chen VB, Arendall 3rd WB, Headd JJ, Keedy DA, Immormino RM, Kapral GJ, Murray LW, Richardson JS and Richardson DC (2010) MolProbity: all-atom structure validation for macromolecular crystallography. *Acta Crystallogr D Biol Crystallogr* **66**, 12–21.
31 Larkin MA, Blackshields G, Brown NP, Chenna R, McGettigan PA, McWilliam H, Valentin F, Wallace IM, Wilm A, Lopez R *et al.* (2007) Clustal W and Clustal X version 2.0. *Bioinformatics* **23**, 2947–2948.
32 Gouet P, Robert X and Courcelle E (2003) ESPript/ENDscript: extracting and rendering sequence and 3D information from atomic structures of proteins. *Nucleic Acids Res* **31**, 3320–3323.
33 Collaborative Computational Project, N (1994) The CCP4 suite: programs for protein crystallography. *Acta Crystallogr D Biol Crystallogr* **50**, 760–763.
34 Rulisek L and Vondrasek J (1998) Coordination geometries of selected transition metal ions (Co^{2+}, Ni^{2+}, Cu^{2+}, Zn^{2+}, Cd^{2+}, and Hg^{2+}) in metalloproteins. *J Inorg Biochem* **71**, 115–127.
35 Saraswat S, Desireddy A, Zheng DS, Guo LJ, Lu HP, Bigioni TP and Isailovic D (2011) Energy transfer from fluorescent proteins to metal nanoparticles. *J Phys Chem C* **115**, 17587–17593.

Supporting information

Additional Supporting Information may be found online in the supporting information tab for this article:
Fig. S1. Reversible quenching effect of the Dronpa by Co^{2+} and Cu^{2+}.
Fig S2. Molecular surface of the Dronpa. EDTA molecule could not access the internal area of the Dronpa β-barrel.
Fig. S3. Electron density map of the (a) Co^{2+}, (b) Ni^{2+}, and (c) Cu^{2+} binding sites.
Fig. S4. Comparison of metal binding structures and their chromophores.
Fig. S5. Comparison of the chromophores and its environment when bound to either (a) Co^{2+} (pink), (b) Ni^{2+} (green) or (c) Cu^{2+} (orange). Asn38, Arg66, Arg91, His193, Glu144, and Glu211 residues showed small conformation changes with metal binding compared with apo-Dronpa (gray).
Fig. S6. Steroview of the metal coordinations of the (a) Co^{2+} and (b) Ni^{2+} on the Dronpa.
Table S1. Quenching effect of metal ions on Dronpa fluorescence**.**
Table S2. Titration of the Dronpa with Co^{2+} and Cu^{2+} ions.
Table S3. Reversibility of the Co^{2+} and Cu^{2+} bound Dronpa by EDTA.
Table S4. Distance between the metal ions and chromophores in Dronpa-metal complexes.
Table S5. The conformational changes of chromophores in Dronpa-metal complex, measured in terms of angle (°) and shift (Å).
Table S6. Distance between the metal ions and chromophores in Dronpa-metal complexes.